PHOTONICS Research

# Integrated heterogeneous silicon/III–V mode-locked lasers

Michael L. Davenport,* Songtao Liu, and John E. Bowers

*Department of Electrical and Computer Engineering, University of California, Santa Barbara, California 93106, USA*
**Corresponding author: mld01@ece.ucsb.edu*

*Received 12 January 2018; revised 12 February 2018; accepted 15 February 2018; posted 16 February 2018 (Doc. ID 318990); published 20 April 2018*

**The mode-locked laser diode has emerged as a promising candidate as a signal source for photonic radar systems, wireless data transmission, and frequency comb spectroscopy. They have the advantages of small size, low cost, high reliability, and low power consumption, thanks to semiconductor technology. Mode-locked lasers based on silicon photonics advance these qualities by the use of highly advanced silicon manufacturing technology. This paper will begin by giving an overview of mode-locked laser diode literature, and then focus on mode-locked lasers on silicon. The dependence of mode-locked laser performance on design details is presented.** 

***OCIS codes:*** (140.4050) Mode-locked lasers; (140.2020) Diode lasers; (250.5300) Photonic integrated circuits.

https://doi.org/10.1364/PRJ.6.000468

## 1. INTRODUCTION

The mode-locked laser is a special class of laser that produces a time-domain series of short optical pulses at radio frequencies. Emission of a short pulse in the time domain will also generate a wide bandwidth in the optical frequency domain. They have a broad range of applications: the pulses have very high peak power due to their short time duration, allowing them to be used for precision medical cutting applications [1]; the resulting comb of optical frequency tones may have octave-spanning bandwidth, allowing generation of ultra-stable microwave signals for use in optical clocks, frequency measurement [2], and broadband spectroscopy [3]; the high timing stability, in combination with very short pulse duration, can be used for all-optical analog-to-digital conversion [4]; and the harmonic series of tones in the microwave frequency domain may be used for signal generation in photonic radar [5].

The mode-locked laser diode is a subset of mode-locked lasers that is based on semiconductor gain media as opposed to bulk crystals, such as Ti:sapphire and Nd:YAG, or doped glass fibers, such as the erbium-doped fiber amplifier (EDFA). The principal advantages of mode-locked laser diodes are their small size and capability for electrical pumping; in contrast, bulk crystal lasers and fiber lasers must be optically pumped, often with laser diodes, which increases the cost and complexity of the system. Optically pumped semiconductor mode-locked lasers also exist, for example, the vertical-external-cavity surface-emitting laser [6], and have demonstrated high peak power and ultra-fast pulses. Electrical pumping of vertical external cavity lasers is also possible [7].

While mode-locked laser diodes do not have high enough peak power or frequency comb bandwidth to be outright competitive with their bulk and fiber laser counterparts, they enjoy the advantages of semiconductor manufacturing technology. This allows for manufacturing large numbers of devices at wafer-scale, and the production of either low-cost discrete devices or the combination of many device functions into larger integrated circuits. This represents the greatest promise of the integrated mode-locked laser diode, as the laser can be combined with passive waveguide filters, multiplexers, demultiplexers, and polarization controllers; intensity and phase modulators; photodetectors; and other lasers, mode-locked, tunable, or otherwise [8].

This advantage has been largely unrealized. Most examples of mode-locked laser diodes in the literature have cleaved facet mirrors and all-active waveguides. An integrated circuit with a mode-locked laser will require a laser with an on-chip mirror, and integration with passive components and modulators requires a transition from the gain section waveguide to a passive waveguide. Therefore, for a mode-locked laser diode to be considered "fully integrated," it requires on-chip mirrors to form the cavity, an active amplifier waveguide, the saturable absorber, a passive waveguide, and a transition from the active waveguide to the passive waveguide. The goal of this work was to integrate all of these components in a single mode-locked laser and then demonstrate state-of-the-art performance compared to non-integrated mode-locked laser diodes.

Toward this goal, there are two widely used material platforms for producing integrated mode-locked lasers. The first,

and most mature, is the monolithic indium phosphide (InP) platform, which typically uses regrowth techniques for integrating devices with different bandgap wavelengths. The second, and more recently emerged, is the heterogeneous silicon/III–V platform, which uses silicon-on-insulator (SOI) to provide passive devices and bonded III–V materials (typically grown on InP substrates) to provide the laser amplifier [9]. We review results from both platforms and then focus on the heterogeneous silicon/III–V platform, which is particularly interesting, because the silicon passive waveguide has lower propagation loss than InP, about 1 order of magnitude in the best case [10,11]. In addition, silicon components are normally more compact, and can leverage the scale and precision of CMOS manufacturing technology for lower cost and higher volume applications.

The quantum well used in the laser amplifier is commonly grown using a quaternary alloy, which allows independent control of the bandgap and lattice constant to attain a specific emission wavelength and compressive strain. The two most common (and currently commercially available) quantum well materials are InGaAsP and AlGaInAs. AlGaInAs was used for the quantum well in this work, because it has been demonstrated to have shorter absorber recovery time than InGaAsP [12] and theorized to have lower linewidth enhancement factor [13].

This paper will be organized as follows. First, a review of existing work in fully integrated mode-locked lasers will be presented to establish the state of the art. Then, we focus on integrated silicon technologies and present the experimental results for the optimization of the various components used in the laser: the active-to-passive transition, the saturable absorber, the amplifier waveguide, the quantum well strain, and the laser cavity mirror. The paper will conclude with a brief discussion of possible avenues for further improved performance.

## 2. MODE-LOCKED LASER REVIEW

This section will present an overview of mode-locked laser diode technologies with regards to the three important figures of merit: the pulse width, the peak power, and the 3-dB-down linewidth of the passively mode-locked radio-frequency (RF) tone. Pulse width was chosen because it is the most widely reported performance aspect of these devices in literature and because it represents the quality of the mode locking, since the minimum optical bandwidth of phase-locked mode comb lines can be inferred from the pulse width through the time–bandwidth limit. The spectral bandwidth itself is a less reliable metric, since the existence of a broad mode comb does not necessarily mean that all of the modes are locked if it is not generating a short pulse. The peak power is used to examine the laser power, and is of particular interest with fully integrated lasers; they often have poor optical efficiency due to excess loss introduced by the integrated components. Note that the continuous wave (CW) power is not particularly useful when comparing mode-locked lasers, since they often produce their shortest pulse only at a particular bias current. The radio-frequency linewidth represents the passive stability of the laser. It is particularly important in applications where an electronic synthesizer for active mode locking is undesirable or unavailable, as in the case of a signal generator for a terahertz transmission system. Residual timing jitter for actively mode-locked lasers is also a useful metric, but it is reported very rarely in literature due to the challenging nature of the measurement, so it will not be covered here.

The majority of the work in literature on mode-locked laser diodes thus far has been at 1.55 μm wavelength, due to the importance of telecommunication applications of mode-locked lasers, also because the manufacturing and design of telecommunications band lasers are well developed. There are some examples of 1.31-μm mode-locked lasers [14], but few fully integrated examples [15]. To avoid complicating the comparisons, this paper will focus on 1.55 μm wavelength lasers.

For the purpose of these comparisons, a "Fabry–Perot mirror" laser is one with cleaved or polished flat facets and a single active amplifier waveguide (which is also used for the saturable absorber). It represents the lowest level of integration. An "integrated mirror" laser has only an active waveguide but has one or both mirrors on the chip. An "integrated waveguide" laser has a second waveguide integrated on the chip, but flat facet mirrors. The second waveguide is often a passive section, but in one case is a butt-joint regrown saturable absorber. "Fully integrated" means that the laser has both an on-chip mirror and an integrated passive waveguide. These cavity designs are shown schematically in Fig. 1.

The list of references for the following literature comparisons is Refs. [16–53].

Figure 2 shows the autocorrelation-extracted pulse width of the selected lasers, plotted versus the repetition rate. With only one exception [52], all sub-1-ps pulses come from lasers with flat facet mirrors. The lowest pulse width shown is a quantum dot laser [17] at 312 fs, and after that is an AlGaInAs quantum well laser with pulse 490 fs and an integrated passive waveguide [19]. Evidently, an integrated passive waveguide may be helpful with the pulse width, but lasers with only integrated mirrors have generally poor performance. Many of them have active distributed Bragg reflector (DBR) mirrors that have limited bandwidth.

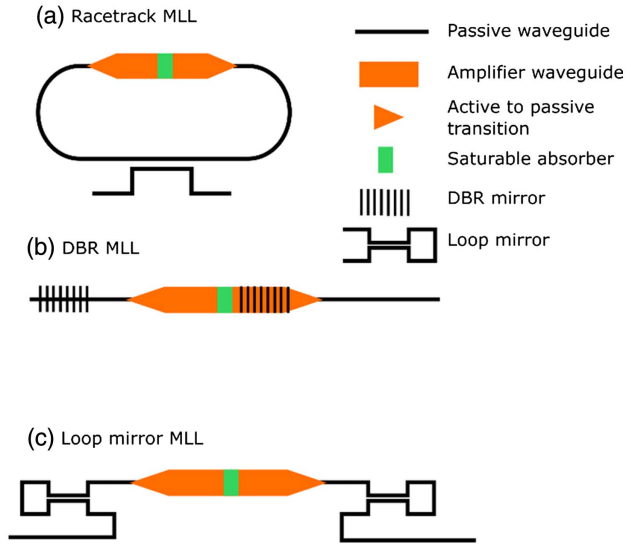


**Fig. 1.** Schematic of the most common forms of fully integrated mode-locked laser cavity designs.

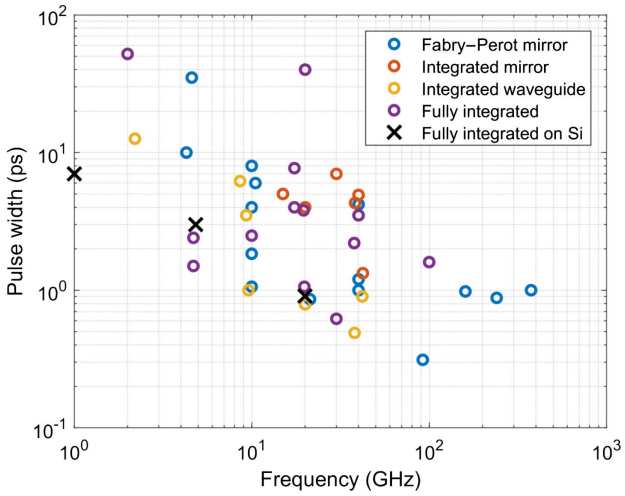


**Fig. 2.** Pulse width of a selection of mode-locked laser diodes from the literature.

Figure 3 shows the peak power of lasers from the literature survey. There is a generally decreasing trend of peak power versus repetition frequency, because the laser CW power is divided up between more pulses at higher frequency. Integrated lasers typically have 6–10 times lower peak power because of the excess loss introduced by the integrated components. The 98 mW peak power of the laser presented in this work, shown as a black "X", is the highest of any fully integrated laser at 20 GHz. One integrated mirror laser, at 40 GHz, beats the trend by integrating a high-power flared amplifier on-chip with the laser [23]. Approximate trend lines are shown, representing the decrease in peak power due to increasing repetition rate. Fully integrated lasers are typically 1 order of magnitude lower in peak power due to excess loss in the integrated components.

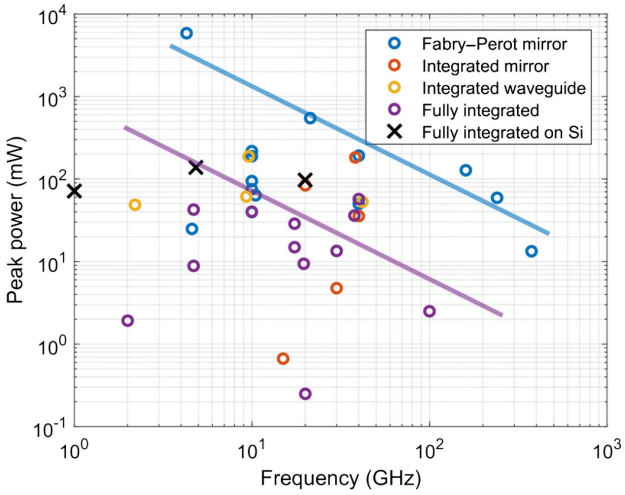


**Fig. 3.** Peak power of a selection of lasers from the literature, including this work. The colored lines represent approximate trends; purple is for fully integrated lasers, and blue is for Fabry–Perot lasers. The silicon lasers were not considered part of the trend.

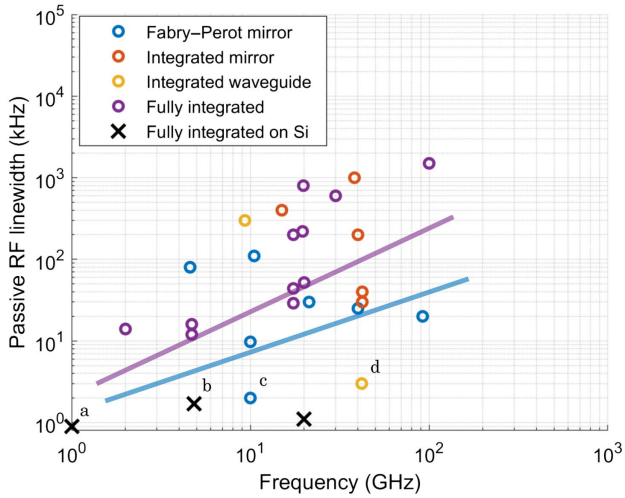


**Fig. 4.** 3 dB passively-mode locked RF linewidth of a selection of mode-locked lasers from the literature. The colored lines represent approximate trends; purple is for fully integrated lasers, and blue is for Fabry–Perot lasers. The silicon lasers and the two labeled outliers were not considered part of the trend.

Figure 4 shows the 3 dB passively mode-locked RF linewidth of lasers from literature. There are comparatively fewer data points on this chart, since this measurement is less commonly performed than autocorrelation. Like peak power, the linewidth generally improves—trending downward—with decreasing frequency. A few notable exceptions to the trend are indicated with superscripts. "a" and "b", like the laser presented in this work, are heterogeneous silicon/InP lasers, specifically with very long cavities formed from low-loss silicon waveguides, which reduces the Schawlow–Townes linewidth, a contributor to the RF linewidth in mode-locked lasers [54]. The laser at "a" reported only its 10 dB linewidth, which is shown in the figure regardless; assuming a Lorentzian line shape, this would correspond to 450 Hz 3 dB linewidth. The laser at "c" uses the AlGaInAs quaternary for its waveguide and quantum well, instead of the much more common InGaAsP. AlGaInAs is reported to have lower linewidth enhancement factor than InGaAsP [13,55], which should reduce the Schawlow–Townes linewidth. The laser at "d" does not have a passive waveguide; instead, it has a butt-joint-regrown uni-traveling-carrier absorber design [30] and displays an impressive 900 fs pulse width as well as the 3 kHz linewidth. Approximate trend lines are shown, with blue representing Fabry–Perot lasers and purple representing fully integrated lasers. The outliers at a, b, c, and d were not considered part of the trend. It is notable that linewidths of the three fully integrated heterogeneous Si lasers are significantly lower than those of the majority of fully integrated devices.

## 3. EXPERIMENT

The laser performance was optimized by producing a standardized test laser in a high-yield fabrication process and then varying individual elements of the design. Thanks to wafer-scale fabrication, many different device designs can be fabricated

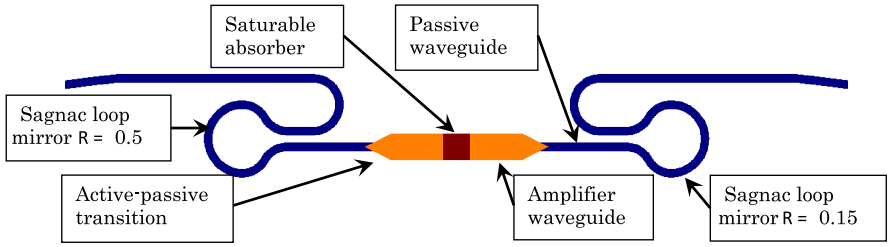


**Fig. 5.** Schematic of the laser test device used in the experimental optimization.

simultaneously on a single die, which helps to increase experimental control. The lasers in Section 3.D, Quantum Well Design, have different quantum well compressive strain, which is accomplished by bonding InP dies with different epitaxial layers to different dies on the SOI substrate and then co-fabricating them. In this way, process variation can be minimized since all devices were fabricated together.

The design of the heterogeneous amplifier section, which is vital to the performance of any laser device, is covered in detail in Ref. [56]. The fabrication process and amplifier cross-section design in this work are identical to in Ref. [56], with the addition of an electrical isolation section between the gain section p-contact and the saturable absorber p-contact. This isolation section is a 1-μm-wide slot wet etched between the two contact pads and then hydrogen implanted, and has a resistance of about 1 kΩ.

An overview schematic of the mode-locked laser is shown in Fig. 5. It consists of a 2-mm-long amplifier waveguide section with two passive waveguides on either side. The amplifier and passive waveguides are connected by an active–passive transition between the heterogeneous amplifier waveguide and the passive waveguide. The passive waveguides are approximately 1 mm in length each, to bring the fundamental cavity free spectral range to 10 GHz, including the amplifier and the loop mirrors. In the center of the amplifier is the saturable absorber, which is typically 60 μm long except when specified otherwise. Placement of the absorber here results in colliding pulse mode locking, so the frequency will be double of the fundamental, or 20 GHz. The laser mirrors are formed by Sagnac loop mirrors [57], which have selectable power reflection from $R = 0$ up to about $R = 0.9$ (limited by propagation loss in the loop) by changing the coupling coefficient of the directional coupler. The cross section of the amplifier waveguide is shown in Fig. 6.

Measurement of the pulse width is performed for each laser across a full range of gain section current and saturable absorber reverse bias. While the lasers make pulses at many bias conditions, the data presented here for each laser will be at the bias condition where the pulse is the shortest. This is typically between 85 and 95 mA gain section current and −4.25 to −4.75 V of saturable absorber bias. Light is collected from the edge of the chip (through a low-reflection angled facet) with a 2-μm-spot-size tapered fiber. The lasers typically lase around 1565 nm wavelength, and so an L-band EDFA is used to amplify the pulse before measurement with an autocorrelator. The pulse width is then determined from fitting a hyperbolic secant squared shape to the autocorrelation function. For the peak power, the lensed fiber is removed and an integrating sphere is

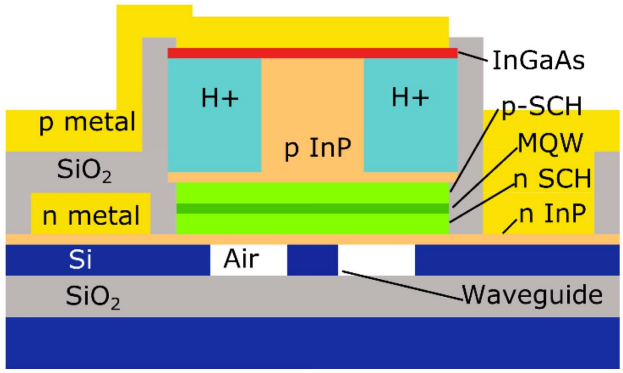


**Fig. 6.** Cross section of the heterogeneous amplifier waveguide. H+ denotes the hydrogen implanted section of the mesa. Current flows down only the central non-implanted p-type InP. The width of the underlying silicon waveguide controls the confinement factor. SCH, separate-confinement heterostructure; MQW, multi-quantum well.

used to measure the CW output power to eliminate uncertainty from fiber-to-chip coupling loss. The output power measurement must be taken with the absorber biased under the exact condition that the shortest pulse was produced, as this will affect the laser slope efficiency.

### A. Heterogeneous Transition

Accomplishing a low parasitic reflection and low insertion loss transition between the active and passive waveguides is critical for producing any high-performance broadband laser. Insertion loss will deteriorate the laser output power, while parasitic reflection creates coupled cavities that limit the laser operating bandwidth. The general concept used for the transition is to use a system of lateral tapers to form essentially a vertical adiabatic coupler. Reduction in loss and reflection of this structure is discussed in Ref. [56]. A large 2-μm-wide and 0.5-μm-thick silicon waveguide is used underneath the tapered III–V mesa to reduce the overlap of the optical mode with the III–V taper, which is lossy. The overall length of the III–V taper is minimized.

For mode-locked lasers, the design in Ref. [56] impaired the performance, because the short III–V taper was not adiabatic. The reflection from the heterogeneous transition measured in Ref. [56] was fairly minimal: −46 dB. Finite-difference time-domain (FDTD) simulation suggests that this was dominated by the thin n-type InP layer termination (−43 dB in FDTD simulation), which was a simple linear taper with a

500-nm-wide tip. This is high compared to −55 dB simulated value for the p-mesa taper. However, the simple 20-μm-long taper in Ref. [56] was not fully adiabatic partially because of the short length and partially because of misalignment between the n-type taper and the silicon waveguide. The resulting higher order mode emission into the multimode silicon waveguide created mode interference and reduced the emission bandwidth. To combat this, a three-section taper design was adopted for the p-mesa taper, where the III–V p-mesa taper remains linear and a single section (for manufacturing simplicity), but the underlying silicon waveguide is tapered in three sections to maintain constant waveguide effective index throughout the transition. The dimensions of the three-section taper are shown in Fig. 7. Note that for all amplifier waveguide widths, the Si waveguide is flared over 80 μm in length from the designed value to $W_{1,si} = 1.35$ μm (see Fig. 7) so that the heterogeneous transition is identical for all devices in that experiment.

Three device comparisons were prepared, using mode-locked lasers with 850-nm-wide Si waveguides in the amplifier section, 0.85% compressive strain quantum wells, 60-μm-long saturable absorbers, and loop mirrors with the 5-μm-radius spline curve bend (see Section 3.E, Loop Mirrors).

The first experiment was to compare a short 15-μm-long taper with a simple straight 2-μm-wide Si waveguide (p, 15 μm basic; n, angle), as in Ref. [56], to the three-section design shown in Fig. 7 (p, 15 μm three-section; n, angle) of the same length. The results are shown in Table 1. The three-section taper reduces the pulse width from 3.5 to 2.7 ps, thanks to reduced higher order mode emission into the wide silicon waveguide from the more gradual mode transformation.

The second comparison is between a short 15-μm-long three-section taper and a longer 30-μm-long three-section taper. This showed a more modest improvement in pulse

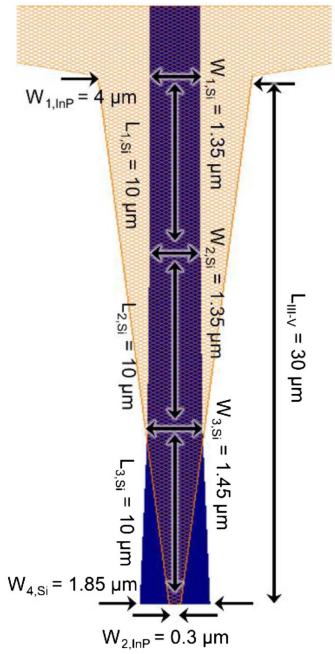


**Fig. 7.** Dimensions of the heterogeneous transition.

**Table 1. Effect of Transition Design on Pulse Width**

| P Transition Style | N Transition Style | Pulse Width (ps) |
|---|---|---|
| 15 μm basic | Taper | 3.45 |
| 15 μm basic | Angle | 2.70 |
| 30 μm conformal | Taper | 2.54 |
| 30 μm conformal | Angle | 2.34 |

width, from 2.7 to 2.6 ps. The two devices had almost identical output power, as the reduction in loss from a more adiabatic transition was offset by the increased absorption from the narrow taper structure.

The third comparison is between the design of the thin n-contact termination. One design uses a taper (p, 30 μm three-section; n, taper), and the other uses an angled transition (p, 30 μm three-section; n, angle). These are shown schematically in Fig. 8. The taper, while superior in simulation, is more difficult to fabricate because of the large topography on the wafer after the p-mesa etch, while the angle has higher reflection in theory but is less sensitive to misalignment and resolution errors. The angled n-layer and three-section 30-μm-long p-mesa taper has the best performance overall, at 2.3 ps, an improvement over the 2.6 ps for the n-layer taper. Optimization of the heterogeneous transition design reduced the pulse width from 3.5 to 2.3 ps.

### B. Saturable Absorber

The length of the absorber is a crucial parameter and can be varied with a lithographic mask dimension in most mode-locked laser designs. Figure 9 shows the impact of the absorber length design in four lasers. The absorber lengths varied from 50 μm (2.5%) to 200 μm (10%). The devices all have 5 μm minimum bend radius spline-curve mirrors, 850 nm waveguides in the amplifier section, 1% compressive strain quantum wells, and 30-μm-long three-section heterogeneous transitions with the angled n-layer. The pulse width decreases with decreasing absorber length, and the data suggests that a 30- or 40-μm-long absorber may have produced an even shorter pulse.

The reason for this behavior is that the longer absorbers have higher loss when compared to shorter absorbers at the same reverse voltage. The long absorbers can prevent multi-mode laser action when biased at lower voltages, whereas the shorter

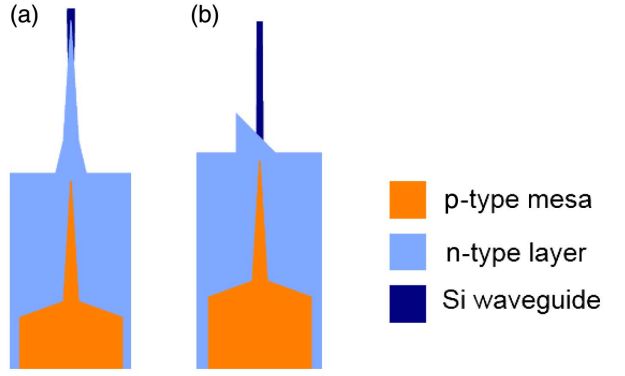


**Fig. 8.** Plan view schematics of the n-type transitions, showing (a) the n-type taper and (b) the n-type angle. In both cases, the p-type transition is the 30 μm three-section taper.

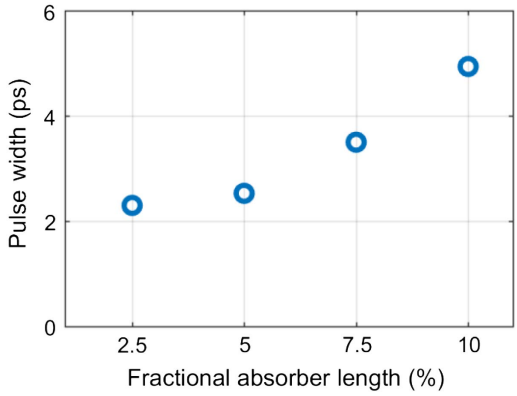


**Fig. 9.** Pulse width versus the absorber length, plotted as a percentage fraction of the gain section length. In this case, with a 2-mm-long gain section, the absorber sections were 50, 100, 150, and 200 μm.

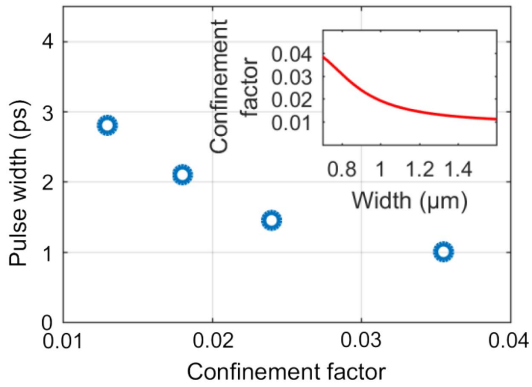


**Fig. 10.** Impact on the pulse width of increasing confinement factor in the pumped current channel region of the quantum well. The quantum well confinement factor is plotted versus waveguide width in the inset.

absorbers can be biased at lower voltage with the same overall loss (due to less length). At lower voltage, the recovery time is reduced, leading to formation of shorter pulses.

### C. Confinement Factor

The optical confinement factor in the active region, both the transverse confinement factor $\Gamma_{xy}$ and the longitudinal confinement factor $\Gamma_z$, can have a strong impact on the pulse width. The shortest on-chip mode-locked laser pulse from a quantum well laser, 490 fs, was produced by exploiting an offset-waveguide three-quantum-well laser with a quantum well intermixed passive waveguide to reduce $\Gamma_z$ [19]. This reduces the impact of self-phase modulation on the pulse broadening.

The heterogeneous silicon waveguides described in this chapter have the capacity to control confinement factor by varying the waveguide width, making straightforward comparisons possible since devices with different confinement factors can be fabricated on the same wafer. Four lasers with 5 μm minimum bend radius spline-curve mirrors with $R = 0.15$ front mirror and $R = 0.5$ rear mirror power reflectivities, 100-μm-long saturable absorbers, 1% compressive quantum wells, and 30-μm-long three-section heterogeneous transitions with the angled n-layer were characterized. For all waveguide designs, there is an 80-μm-long flare from the designed waveguide width to the same waveguide width at the beginning of the heterogeneous transition, 1.35 μm. This ensures that all of the devices have identical transition design. The impact of the flare is expected to be minimal, as it has very low loss (<0.1 dB) in simulation and is relatively short compared to the 2 mm overall length of the amplifier. The pulse width attained from the four devices is shown in Fig. 10. Increasing confinement factor yields a shorter pulse. Based on this, it appears that the pulse width is limited by low amplification at the high-power peak of the pulse. The impact of varying the waveguide width on the quantum well confinement factor is shown in the inset of Fig. 10.

### D. Quantum Well Design

Quantum well design can have a significant impact on laser performance. It primarily affects the lasing wavelength, but, in addition, compressive strain in the well affects both the loss [58] and the linewidth enhancement factor [59]. The hole well is shallower for AlGaInAs wells than InGaAsP wells due to the higher conduction band offset in the AlGaInAs system. Since the conduction band lineup is affected by strain, it may be presumed that there is an optimal compressive strain value beyond which the confinement of holes in the well may be compromised. For that reason, three quantum well designs with different values of compressive strain were designed and used to fabricate mode-locked lasers.

The three devices have 5 μm minimum bend radius spline-curve mirrors with $R = 0.15$ for the front mirror and $R = 0.5$ for the rear mirror (both power reflection), 60-μm-long saturable absorbers, and 30-μm-long three-section heterogeneous transitions with the angled n-layer. The results of the pulse width measurement are shown in Fig. 11. The pulse width initially decreases rapidly from 0.85% to 1% strain, from 2.34 to 1.45 ps, then more modestly from 1.45 to 1.21 ps. This is due to decreased carrier-dependent loss in the more highly strained quantum wells, which has the effect of increasing the differential gain. As suggested by Fig. 10, low gain may limit the pulse width, so an increase in the differential gain is helpful. It does not appear from Fig. 11 that further increase in strain will produce significantly shorter pulse widths.

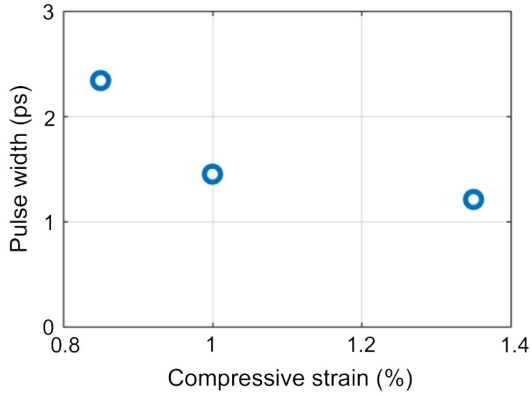


**Fig. 11.** Pulse width versus the quantum well compressive strain in the active region.

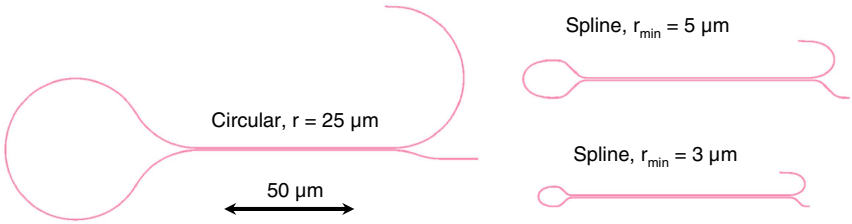


**Fig. 12.** Size comparison of the circular-bend loop mirror and the two spline-curve loop mirrors.

### E. Loop Mirrors

The loop mirror uses a fully etched (down to the buried oxide) directional coupler to increase its resilience to fabrication variation, since a partially etched directional coupler will experience a large change in coupling coefficient based on a small variation in etch depth. To attain high coupling without excessive length or an extremely small coupler gap, the waveguide must then be narrow to expand the mode out into the cladding. The waveguide geometry chosen for the loop mirror component is a 400-nm-wide and 500-nm-tall deeply etched wire waveguide, with a 400 nm gap. The resulting waveguide has a small number of higher order modes and fairly high propagation loss (10 dB/cm). Bend-to-straight transitions cause insertion loss and can excite higher order modes, which then cause mode-beating interference and impair the mode comb bandwidth. These effects are reduced by increasing the bend radius, but this requires a larger length of waveguide and is undesirable in this case due to the high loss.

To mitigate these effects, an adiabatic bend was adopted, using the method described in Ref. [60]. A third-order Bezier spline curve is used to gradually transform the mode into a bend mode, which then propagates through part of the bend in a circular section to reduce the footprint; fully adiabatic bends are normally much larger than a circular bend with the same minimum bend radius. Three mirror designs were chosen: a 25-μm-radius fully circular bend (the radius at which the bent-to-straight transition becomes negligible for this waveguide geometry), a spline-curve bend with a 5-μm-minimum bend radius, and a spline-curve bend with a 3-μm-minimum bend radius. The spline curves use 5- and 3-μm control points and cover 10° of the curve on either side with the spline bend. The s-bends use the spline-circular curve and the u-turn uses a natural spline.

Figure 12 shows a to-scale plan-view image of the three mirrors. Not including the directional coupler (which varies in length depending on the desired mirror reflectivity), the propagation distance in the circular mirror is 217 μm, and has 0.2 dB of loss from 11 curved-to-straight and curved-to-curved transitions, for 0.417 dB of loss per mirror, almost 1 dB in total for both mirrors. In simulation, the spline bend did not display any transition loss. The 5-μm-bend mirror has a propagation length of 57 μm, and the 3-μm-bend mirror has only 30 μm of propagation, translating to 0.057 and 0.03 dB per mirror. The impact of the reduced loss on the laser output power can be seen in Fig. 13. The 3-μm-bend mirror has nearly doubled the maximum output power of the circular bend mirror. Note that all three lasers are designed to have the same $R = 0.5$ rear mirror power reflection and $R = 0.15$ front mirror power reflection.

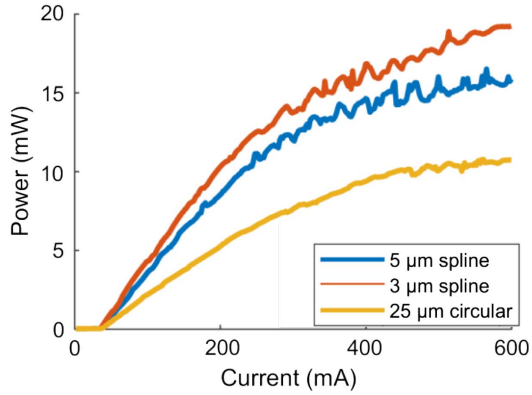


**Fig. 13.** LI characteristic of the three loop mirror split lasers, with the absorbers forward biased at the same current density as the gain sections.

In addition to high propagation loss, the waveguide supports the TE10 and TE01 higher order modes, which can be excited by the heterogeneous transition, as described in Section 4. The very small bend radius attainable with low loss using the spline curve can serve as a mode filter. Figure 14 shows a simulation of the bend loss for the three guided modes in the 400-nm-wide and 500-nm-thick Si waveguide. The TE10 mode is filtered strongly by the 3 μm bends. The 15 μm of propagation in 3-μm-bent waveguides introduces 4 dB of loss in the TE01 mode and 28 dB of loss in the TE10 mode per mirror, according to Fig. 14.

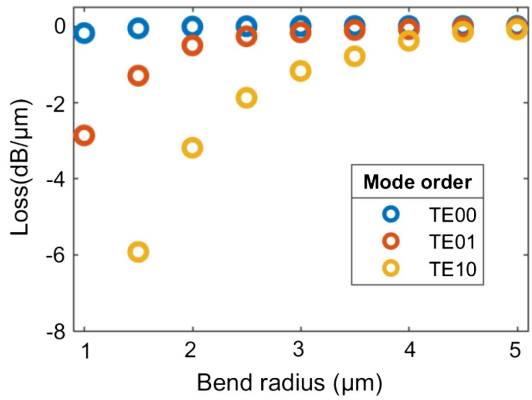


**Fig. 14.** Simulated bend loss for the narrow 400-nm-wide and 500-nm-tall waveguide used for the directional coupler and loop mirror.

This mode filtering effect is helpful for reducing the pulse width. The results of the pulse width measurements are shown in Fig. 15. The 3-μm-bend spline curve mirror has the shortest pulse, at 900 fs, the shortest ever for a mode-locked laser on a silicon substrate, to the best of our knowledge, and the second shortest pulse from any fully integrated mode-locked laser, after Ref. [52]. The autocorrelation trace is shown in Fig. 16, showing a good fit with the $\mathrm{sech}^2$ pulse shape.

The 5-μm-bend mirror was then examined for its passive RF linewidth. To conduct this measurement, the pulse train was detected on a high-speed photodiode, and the resulting electrical signal was inspected using an electrical spectrum analyzer (ESA). The device was powered with a battery current source, which is disconnected from the wall power socket to minimize line noise, and the absorber was biased with a linearized regulated voltage supply. Even though only DC signals were applied to the absorber, it was probed with a 67 GHz ground–signal–ground probe and biased with a 67 GHz bias to avoid impedance-mismatch-related reflections of the higher order microwave harmonics that were generated as electrical signals at the absorber. The device was placed inside of a vibration isolating box and allowed to reach equilibrium temperature while biased without the use of a thermoelectric cooler.

The resulting RF linewidth is shown in Fig. 17, along with a Voigt fit. The linewidth measured directly from the data is 1.1 kHz, the lowest at 20 GHz repetition rate, considerably lower than the trends shown in Fig. 4, and the second-lowest ever reported, after Ref. [53]. The 3-μm-bend mirror had a linewidth of 1.6 kHz. It is unclear if the difference is related to the design of the devices or simply measurement precision. The circular mirror linewidth was 4 kHz. A closer look at the peak of the RF tone is shown in Fig. 18. Side peaks at 2 and 4 kHz can be seen. It is unclear whether these are due to technical noise or if they are intrinsic to the laser. Figure 19 shows the optical spectrum as the laser was emitting a 900 fs pulse. There is 2.96 nm of optical bandwidth, corresponding to a 3.2 time–bandwidth product, which is practically transform limited for a $\mathrm{sech}^2$ pulse (the transform limit is 0.314).

Figure 20 shows the LI characteristic under −4.5 V, with 1.78 mW at 88 mA of bias current (the conditions that

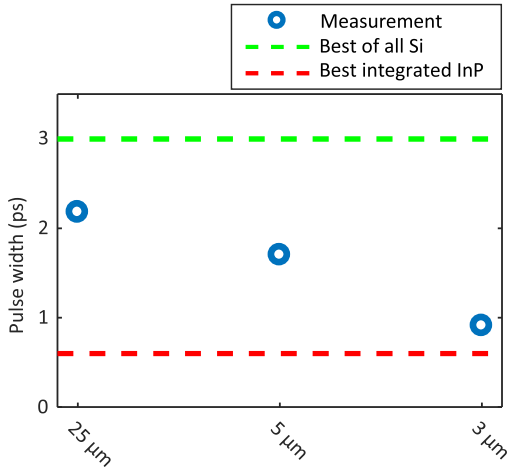


**Fig. 15.** Pulse width versus loop mirror minimum bend radius. The 25-μm-bend mirror has fully circular bends. The 5-μm- and 3-μm-bend mirrors have the spline curve. The 3-μm-bend mirror resulted in the shortest pulse from the entire study, at 900 fs. The "Best integrated InP" result refers to Ref. [52], and the "Best of all Si" result refers to [34].

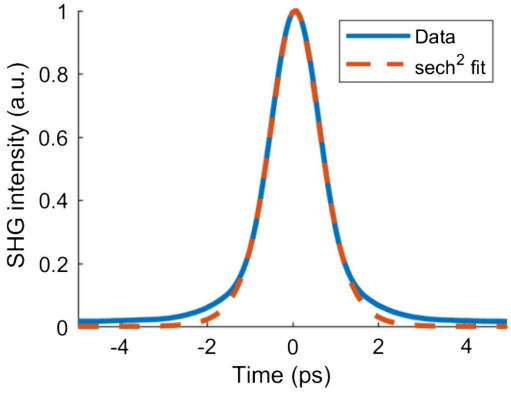


**Fig. 16.** Autocorrelation trace (blue) and $\mathrm{sech}^2$ fit (red dashes) of the 3-μm-bend spline-curve-mirror laser producing a 900 fs pulse.

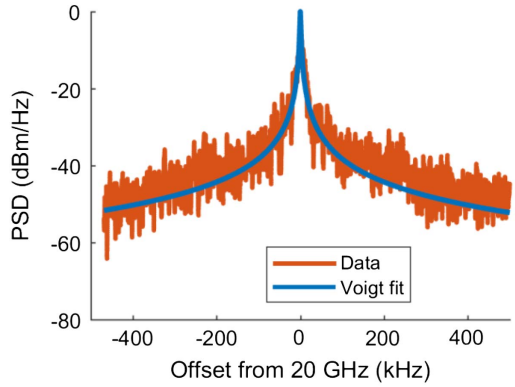


**Fig. 17.** RF tone from the 5-μm-bend spline curve mirror laser (red) and Voigt fit (blue), showing 1.1 kHz linewidth.

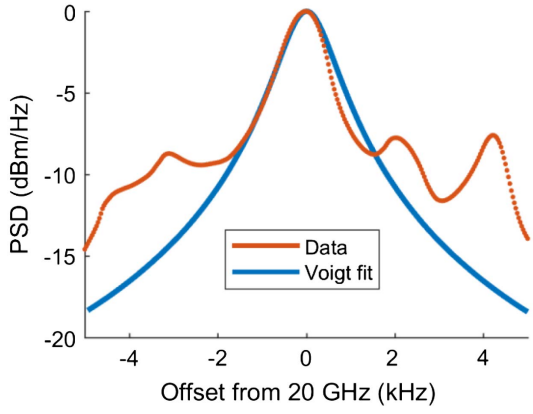


**Fig. 18.** Close-in view of the RF tone from the 5-μm-bend spline curve mirror laser showing the 1.1 kHz, 3 dB linewidth, along with some spurs at 2 and 4 kHz offset.

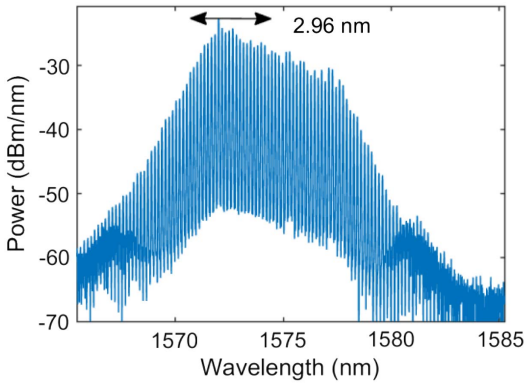


**Fig. 19.** Optical spectrum from the 3-μm-bend spline curve mirror laser while it was producing the 900 fs pulse. The 3-dB bandwidth of the comb is 2.96 nm.

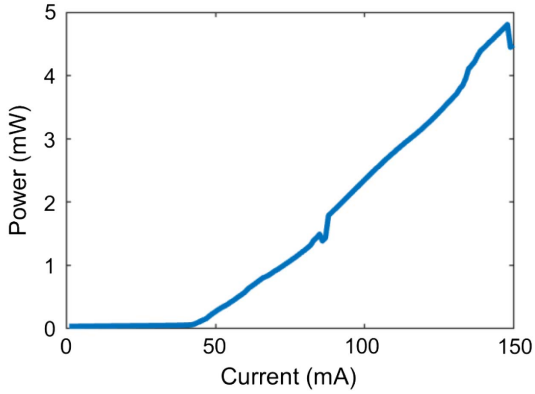


**Fig. 20.** LI characteristic from the 3-μm-bend laser under −4.5 V reverse bias. The shortest pulse came at 89 mA bias current, when the CW power was 1.83 mW. This corresponds to 98 mW peak power.

produced the shortest pulse). This corresponds to 98 mW of peak power.

## 4. CONCLUSIONS

The heterogeneous silicon/III–V platform has recently emerged as the most promising candidate for the realization of high-performance fully integrated mode-locked laser diodes for use as generators of short pulses, microwave carrier signals, and dense frequency combs. This is due to material advantages enjoyed by silicon waveguides and sophisticated silicon fabrication technology.

We have presented here a thorough experimental optimization of a heterogeneous silicon/III–V mode-locked laser for short pulses, demonstrating a 900 fs pulse from the best device, the shortest ever for a mode-locked laser on a silicon substrate. In addition, this structure showed 1.1 kHz passively mode-locked RF linewidth, the lowest ever demonstrated at 20 GHz, and peak power of 98 mW, the highest from any fully integrated laser around 20 GHz repetition rate. These lasers are fully integrated, meaning that all the laser components are on the chip, allowing the device to be added to an integrated circuit without compromising its performance, so long as the parasitic effects from devices along the same waveguide are properly managed.

In addition, the data in this study counters a commonly held notion that reducing the active region confinement factor improves pulse width due to reduced gain saturation and self-phase modulation, by using the special capability of this style of heterogeneous amplifier to produce mode-locked lasers with various confinement factors on a single chip. The tightly controlled experiment showed a clearly increasing trend of pulse width as the confinement factor decreased (Fig. 10).

Further increasing the confinement factor by reducing the waveguide width will increase the propagation loss as the modal overlap with p-doped InP layers increases. It may instead be more practical to increase the longitudinal confinement factor $\Gamma_z$, by lengthening the gain section relative to the overall cavity length. This could reduce the pulse width, as the 900 fs pulse result with the 3-μm-bend mirror used the 850-nm-wide waveguide (2.4%), and the confinement factor study in Fig. 10 used the 5-μm-bend mirror. Combination of the highest confinement factor (3.5%) 700 nm waveguide with the best performing spline mirror should produce a shorter pulse.

A simple modification to the mirror design could increase the power by as much as a factor of 2. All the lasers presented so far use a power reflection $R = 0.15$ front mirror and $R = 0.5$ rear mirror. A separate laser with front-mirror reflection of $R = 0.04$ nearly doubled the slope efficiency, resulting in a maximum output power of 38 mW. This laser did not have a saturable absorber, but compared to the lasers in Fig. 13, the output power is nearly doubled. This laser has the highest CW output power of any heterogeneous silicon/III–V laser reported so far, and is comparable with InP-substrate integrated lasers. This design change, provided that it does not perturb the pulse width, could result in peak power of 200 mW. This is still considerably lower than the best 20 GHz cleaved-facet Fabry–Perot mode-locked laser peak power result of 540 mW [29] because of parasitic losses introduced by the active-to-passive transition, passive waveguides, mirrors, and routing waveguides leading to the output facet. Reducing these losses will be critical for closing the gap between fully integrated and Fabry–Perot mode-locked laser performance.

Dispersion compensation is a common technique in femtosecond bulk crystal lasers, and it should be valuable in a mode-locked laser diode, as all the waveguides are normally dispersive. The introduction of a waveguide with anomalous dispersion inside the cavity could be a pathway to a shorter pulse. Narrow silicon waveguides (narrower than they are tall) can have anomalous dispersion; however, they also have high loss. Integration with a passive silicon nitride waveguide, such as in Ref. [61], could be a way to include dispersion compensation inside the cavity without elevating the loss.

**Funding.** Defense Advanced Research Projects Agency (DARPA) EPHI and DODOS contracts.

**Acknowledgment.** The authors thank Nick Usechek of AFRL and Tin Komljenovic and Larry Coldren of UCSB for helpful discussions.

## REFERENCES


1. F. Dausinger and S. Nolte, *Femtosecond Technology for Technical and Medical Applications*, Vol. **96** of Topics in Applied Physics (Springer, 2004).
2. J. L. Hall, "Optical frequency measurement: 40 years of technology revolutions," IEEE J. Sel. Top. Quantum Electron. **6**, 1136–1144 (2000).
3. W. Coddington, I. Newbury, and N. Swann, "Dual-comb spectroscopy," Optica **3**, 414–426 (2016).
4. P. T. Callahan, M. L. Dennis, and T. R. Clark, Jr., "Photonic analog-to-digital conversion," Johns Hopkins APL Tech. Dig. **30**, 280–286 (2012).
5. P. Ghelfi, F. Laghezza, F. Scotti, G. Serafino, A. Capria, S. Pinna, D. Onori, C. Porzi, M. Scaffardi, A. Malacarne, V. Vercesi, E. Lazzeri, F. Berizzi, and A. Bogoni, "A fully photonics-based coherent radar system," Nature **507**, 341–345 (2014).
6. U. Keller and A. C. Tropper, "Passively modelocked surface-emitting semiconductor lasers," Phys. Rep. **429**, 67–120 (2006).
7. W. Jiang, M. Shimizu, R. P. Mirin, T. E. Reynolds, and J. E. Bowers, "Electrically pumped mode-locked vertical-cavity semiconductor lasers," Opt. Lett. **18**, 1937–1939 (1993).
8. M. Smit, X. Leijtens, H. Ambrosius, E. Bente, J. van der Tol, B. Smalbrugge, T. de Vries, E.-J. Geluk, J. Bolk, R. van Veldhoven, L. Augustin, P. Thijs, D. D'Agostino, H. Rabbani, K. Lawniczuk, S. Stopinski, S. Tahvili, A. Corradi, E. Kleijn, D. Dzibrou, M. Felicetti, E. Bitincka, V. Moskalenko, J. Zhao, R. Santos, G. Gilardi, W. Yao, K. Williams, P. Stabile, P. Kuindersma, J. Pello, S. Bhat, Y. Jiao, D. Heiss, G. Roelkens, M. Wale, P. Firth, F. Soares, N. Grote, M. Schell, H. Debregeas, M. Achouche, J.-L. Gentner, A. Bakker, T. Korthorst, D. Gallagher, A. Dabbs, A. Melloni, F. Morichetti, D. Melati, A. Wonfor, R. Penty, R. Broeke, B. Musk, and D. Robbins, "An introduction to InP-based generic integration technology," Semicond. Sci. Technol. **29**, 83001 (2014).
9. T. Komljenovic, M. Davenport, J. Hulme, A. Y. Liu, C. T. Santis, A. Spott, S. Srinivasan, E. J. Stanton, C. Zhang, and J. E. Bowers, "Heterogeneous silicon photonic integrated circuits," J. Lightwave Technol. **34**, 20–35 (2015).
10. A. Bhardwaj, M. Larson, M. Moewe, and Y. Feng, "Low-loss InGaAsP/InP surface ridge waveguides for photonic integrated circuits," IEEE Photon. Technol. Lett. **28**, 1403–1405 (2016).
11. A. Biberman, M. J. Shaw, E. Timurdogan, J. B. Wright, and M. R. Watts, "Ultralow-loss silicon ring resonators," Opt. Lett. **37**, 39–41 (2012).
12. R. P. Green, M. Haji, L. Hou, G. Mezosi, R. Dylewicz, and A. E. Kelly, "Fast saturable absorption and 10 GHz wavelength conversion in Al-quaternary multiple quantum wells," Opt. Express **19**, 9737–9743 (2011).
13. D. P. Sapkota, M. S. Kayastha, and K. Wakita, "Analysis of linewidth enhancement factor for compressively strained AlGaInAs and InGaAsP quantum well lasers," Opt. Quantum Electron. **45**, 35–43 (2013).
14. J. E. Bowers, P. A. Morton, A. Mar, and S. W. Corzine, "Actively mode-locked semiconductor lasers," IEEE J. Quantum Electron. **25**, 1426–1439 (1989).
15. D. J. Derickson, R. J. Helkey, A. Mar, J. R. Karin, J. G. Wasserbauer, and J. E. Bowers, "Short pulse generation using multisegment mode-locked semiconductor lasers," IEEE J. Quantum Electron. **28**, 2186–2202 (1992).
16. L. Hou, M. Haji, J. H. Marsh, and A. C. Bryce, "10 GHz AlGaInAs/InP 1.55 μm passively mode-locked laser with low divergence angle and timing jitter," in *Conference on Lasers and Electro-Optics (CLEO)* (2011), paper Mo.1.LeSaleve.2.
17. Z. G. Lu, J. R. Liu, S. Raymond, P. J. Poole, P. J. Barrios, and D. Poitras, "312-fs pulse generation from a passive C-band InAs/InP quantum dot mode-locked laser," Opt. Express **16**, 10835–10840 (2008).
18. M. Dontabactouny, C. Rosenberg, E. Semenova, D. Larsson, K. Yvind, R. Piron, F. Grillot, O. Dehaese, N. Chevalier, and S. Loualiche, "10-GHz 1.59-μm quantum dash passively mode-locked two-section lasers," Proc. SPIE **7720**, 77201A (2010).
19. L. Hou, M. Haji, J. H. Marsh, and A. C. Bryce, "490 fs pulse generation from a passive C-band AlGaInAs/InP quantum well mode-locked laser," Opt. Lett. **37**, 773–775 (2012).
20. L. Hou, M. Haji, J. Akbar, B. Qiu, and A. C. Bryce, "Low divergence angle and low jitter 40 GHz AlGaInAs/InP 1.55 μm mode-locked lasers," Opt. Lett. **36**, 966–968 (2011).
21. C. Ji, N. Chubun, R. G. Broeke, J. Cao, Y. Du, S. J. B. Yoo, K. Y. Liou, J. R. Lothian, S. Vatanapradit, S. N. G. Chu, B. Patel, W. S. Hobson, and W. T. Tsang, "Synchronized transform-limited operation of 10-GHz colliding pulse mode-locked laser," IEEE Photon. Technol. Lett. **18**, 625–627 (2006).
22. J. F. Martins-Filho, E. A. Avrutin, C. N. Ironside, and J. S. Roberts, "Monolithic multiple colliding pulse mode-locked quantum-well lasers: experiment and theory," IEEE J. Sel. Top. Quantum Electron. **1**, 539–551 (1995).
23. J. Akbar, L. Hou, M. Haji, M. J. Strain, J. H. Marsh, A. C. Bryce, and A. E. Kelly, "High power (130 mW) 40 GHz 1.55 μm mode-locked distributed Bragg reflector lasers with integrated optical amplifiers," Opt. Lett. **37**, 344–346 (2012).
24. S. Keyvaninia, S. Uvin, M. Tassaert, Z. Wang, X. Fu, S. Latkowski, J. Marien, L. Thomassen, F. Lelarge, G. Duan, G. Lepage, P. Verheyen, J. Van Campenhout, E. Bente, and G. Roelkens, "III-V-on-silicon anti-colliding pulse-type mode-locked laser," Opt. Lett. **40**, 3057–3060 (2015).
25. L. Hou, M. Haji, J. Akbar, A. C. Bryce, and J. H. Marsh, "160-GHz 1.55-um colliding-pulse mode-locked AlGaInAs/InP laser with high power and low divergence angle," IEEE Photon. Technol. Lett. **24**, 1057–1059 (2012).
26. L. Hou, M. Haji, and J. H. Marsh, "240 GHz pedestal-free colliding-pulse mode-locked laser with a wide operation range," Laser Phys. Lett. **11**, 115804 (2014).
27. D. Larsson, K. Yvind, and J. M. Hvam, "Wide-band residual phase-noise measurements on 40-GHz monolithic mode-locked lasers," IEEE Photon. Technol. Lett. **17**, 2388–2390 (2005).
28. M. J. R. Heck, A. Renault, E. A. J. M. Bente, Y.-S. Oei, M. K. Smit, K. S. E. Eikema, W. Ubachs, S. Anantathanasarn, and R. Notzel, "Passively mode-locked 4.6 and 10.5 GHz quantum dot laser diodes around 1.55 um with large operating regime," IEEE J. Sel. Top. Quantum Electron. **15**, 634–643 (2009).
29. K. Merghem, A. Akrout, A. Martinez, G. Moreau, J.-P. Tourrenc, F. Lelarge, F. Van Dijk, G. Duan, G. Aubin, and A. Ramdane, "Short pulse generation using a passively mode locked single InGaAsP/InP quantum well laser," Opt. Express **16**, 10675–10683 (2008).
30. R. Scollo, H.-J. Lohe, F. Robin, D. Erni, E. Gini, and H. Jackel, "Mode-locked InP-based laser diode with a monolithic integrated UTC absorber for subpicosecond pulse generation," IEEE J. Quantum Electron. **45**, 322–335 (2009).
31. J. H. Marsh, F. Camacho, E. A. Avrutin, and A. C. Bryce, "Passive modelocking in semiconductor lasers with monolithically integrated passive waveguides," IEEE Proc. J. Optoelectron. **145**, 43–46 (1998).
32. P. B. Hansen, G. Raybon, U. Koren, B. I. Miller, M. G. Young, M. A. Newkirk, M.-D. Chien, B. Tell, and C. A. Burrus, "2 cm long monolithic multisection laser for active modelocking at 2.2 GHz," Electron. Lett. **29**, 739–741 (1993).
33. P. B. Hansen, G. Raybon, U. Koren, P. P. Iannone, B. I. Miller, G. M. Young, M. A. Newkirk, and C. A. Burrus, "InGaAsP monolithic extended-cavity lasers with integrated saturable absorbers for active, passive, and hybrid mode locking at 8.6 GHz," Appl. Phys. Lett. **62**, 1445–1447 (1993).
34. L. Hou, M. Haji, B. Qiu, and A. C. Bryce, "Mode-locked laser array monolithically integrated with MMI combiner, SOA, and EA modulator," IEEE Photon. Technol. Lett. **23**, 1064–1066 (2011).
35. H. Fan, C. Wu, M. El-Aasser, N. K. Dutta, U. Koren, and A. B. Piccirilli, "Colliding pulse mode-locked laser," IEEE Photon. Technol. Lett. **12**, 972–973 (2000).
36. M. S. Tahvili, Y. Barbarin, X. J. M. Leijtens, T. de Vries, E. Smalbrugge, J. Bolk, H. P. M. M. Ambrosius, M. K. Smit, and E. A. J. M. Bente, "Directional control of optical power in integrated InP/InGaAsP extended cavity mode-locked ring lasers," Opt. Lett. **36**, 2462–2464 (2011).

37. S. Joshi, C. Calò, N. Chimot, M. Radziunas, R. Arkhipov, S. Barbet, A. Accard, A. Ramdane, and F. Lelarge, "Quantum dash based single section mode locked lasers for photonic integrated circuits," Opt. Express **22**, 11254–11266 (2014).
38. S. Joshi, N. Chimot, R. Rosales, S. Barbet, A. Accard, A. Ramdane, and F. Lelarge, "Mode locked InAs/InP quantum dash based DBR laser monolithically integrated with a semiconductor optical amplifier," in *International Conference on Indium Phosphide and Related Materials (IPRM)* (2013).
39. L. Hou, M. Haji, and J. H. Marsh, "Monolithic mode-locked laser with an integrated optical amplifier for low-noise and high-power operation," IEEE J. Sel. Top. Quantum Electron. **19**, 1100808 (2013).
40. A. W. Fang, B. R. Koch, K.-G. Gan, H. Park, R. Jones, O. Cohen, M. J. Paniccia, D. J. Blumenthal, and J. E. Bowers, "A racetrack mode-locked silicon evanescent laser," Opt. Express **16**, 1393–1398 (2008).
41. S. Srinivasan, A. Arrighi, M. J. R. Heck, J. Hutchinson, E. Norberg, G. Fish, and J. E. Bowers, "Harmonically mode-locked hybrid silicon laser with intra-cavity filter to suppress supermode noise," IEEE J. Sel. Top. Quantum Electron. **20**, 8–15 (2014).
42. B. R. Koch, A. W. Fang, O. Cohen, and J. E. Bowers, "Mode-locked silicon evanescent lasers," Opt. Express **15**, 11225–11233 (2007).
43. S. Srinivasan, E. Norberg, T. Komljenovic, M. Davenport, G. Fish, and J. E. Bowers, "Hybrid silicon colliding-pulse mode-locked lasers with on-chip stabilization," IEEE J. Sel. Top. Quantum Electron. **21**, 24–29 (2015).
44. S. Keyvaninia, S. Uvin, M. Tassaert, X. Fu, S. Latkowski, J. Mariën, L. Thomassen, F. Lelarge, G. Duan, P. Verheyen, G. Lepage, J. Van Campenhout, E. Bente, and G. Roelkens, "Narrow-linewidth short-pulse III-V-on-silicon mode-locked lasers based on a linear and ring cavity geometry," Opt. Express **23**, 3221–3229 (2015).
45. Y. Barbarin, E. A. J. M. Bente, M. J. R. Heck, Y. S. Oei, R. Nötzel, and M. K. Smit, "Characterization of a 15 GHz integrated bulk InGaAsP passively modelocked ring laser at 1.53 μm," Opt. Express **14**, 9716–9727 (2006).
46. V. Moskalenko, S. Latkowski, S. Tahvili, T. de Vries, M. Smit, and E. Bente, "Record bandwidth and sub-picosecond pulses from a monolithically integrated mode-locked quantum well ring laser," Opt. Express **22**, 28865–28874 (2014).
47. S. Arahira, Y. Katoh, and Y. Ogawa, "20 GHz subpicosecond monolithic modelocked laser diode," Electron. Lett. **36**, 454–456 (2000).
48. R. Kaiser, B. Huttl, H. Heidrich, S. Fidorra, W. Rehbein, H. Stolpe, R. Stenzel, W. Ebert, and G. Sahin, "Tunable monolithic mode-locked lasers on InP with low timing jitter," IEEE Photon. Technol. Lett. **15**, 634–636 (2003).
49. K. Sato, I. Kotaka, Y. Kondo, and M. Yamamoto, "Actively mode-locked strained-InGaAsP multiquantum-well lasers integrated with electroabsorption modulators and distributed Bragg reflectors," IEEE J. Sel. Top. Quantum Electron. **2**, 557–565 (1996).
50. S. Arahira, Y. Matsui, T. Kunii, S. Oshiba, and Y. Ogawa, "Transform-limited optical short-pulse generation at high repetition rate over 40 GHz from a monolithic passive mode-locked DBR laser diode," IEEE Photon. Technol. Lett. **5**, 1362–1365 (1993).
51. J. J. Plant, J. T. Gopinath, B. Chann, D. J. Ripin, R. K. Huang, and P. W. Juodawlkis, "250 mW, 1.5 m monolithic passively mode-locked slab-coupled optical waveguide laser," Opt. Lett. **31**, 223–225 (2006).
52. J. S. Parker, A. Bhardwaj, P. R. A. Binetti, Y. Hung, C. H. Lin, and L. A. Coldren, "Integrated 30 GHz passive ring mode-locked laser with gain flattening filter," in *IEEE International Semiconductor Laser Conference (ISLC)* (2010), pp. 3–4.
53. Z. Wang, K. Van Gasse, V. Moskalenko, S. Latkowski, E. Bente, B. Kuyken, and G. Roelkens, "A III-V-on-Si ultra-dense comb laser," Light Sci. Appl. **6**, e16260 (2017).
54. F. Kéfélian, S. O'Donoghue, M. T. Todaro, J. G. McInerney, and G. Huyet, "RF linewidth in monolithic passively mode-locked semiconductor laser," IEEE Photon. Technol. Lett. **20**, 1405–1407 (2008).
55. J. Minch, S. H.-H. Park, T. Keating, and S. L.-L. Chuang, "Theory and experiment of InGaAsP and InGaAlAs long-wavelength strained quantum-well lasers," IEEE J. Quantum Electron. **35**, 771–782 (1999).
56. M. L. Davenport, S. Skendzic, N. Volet, J. C. Hulme, M. J. R. Heck, and J. E. Bowers, "Heterogeneous silicon/III-V semiconductor optical amplifiers," IEEE J. Sel. Top. Quantum Electron. **22**, 78–88 (2016).
57. X. Sun, L. Zhou, J. Xie, Z. Zou, L. Lu, H. Zhu, X. Li, and J. Chen, "Tunable silicon Fabry–Perot comb filters formed by Sagnac loop mirrors," Opt. Lett. **38**, 567–569 (2013).
58. G. Fuchs, J. Hörer, A. Hangleiter, V. Härle, F. Scholz, R. W. Glew, and L. Goldstein, "Intervalence band absorption in strained and unstrained InGaAs multiple quantum well structures," Appl. Phys. Lett. **60**, 231–233 (1992).
59. L. F. Tiemeijer, P. J. A. Thijs, P. J. de Waard, J. J. M. Binsma, and T. V. Dongen, "Dependence of polarization, gain, linewidth enhancement factor, and K factor on the sign of the strain of InGaAs/InP strained-layer multiquantum well lasers," Appl. Phys. Lett. **58**, 2738–2740 (1991).
60. W. Bogaerts and S. K. Selvaraja, "Compact single-mode silicon hybrid rib/strip waveguide with adiabatic bends," IEEE Photon. J. **3**, 422–432 (2011).
61. M. Piels, J. F. Bauters, M. L. Davenport, M. J. R. Heck, and J. E. Bowers, "Low-loss silicon nitride AWG demultiplexer heterogeneously integrated with hybrid III-V/silicon photodetectors," J. Lightwave Technol. **32**, 817–823 (2014).